

Nonlinear absorption of high-power microwave pulses in a plasma filled waveguide

Cite as: Phys. Plasmas **28**, 062307 (2021); doi: 10.1063/5.0052963

Submitted: 2 April 2021 · Accepted: 23 May 2021 ·

Published Online: 15 June 2021



View Online



Export Citation



CrossMark

Y. Cao,^{a)} J. G. Leopold, Yu. P. Bliokh, G. Leibovitch, and Ya. E. Krasik

AFFILIATIONS

Physics Faculty, Technion, Israel Institute of Technology, Haifa 3200003, Israel

^{a)} Author to whom correspondence should be addressed: neo.cao.yang@gmail.com

ABSTRACT

We observe complete absorption of an ~ 1.2 GW, 0.5 ns, 25.6 GHz high power microwave pulse propagating in a plasma-filled waveguide when the plasma density dependent waveguide cutoff frequency is close to the pulse frequency. Some of the plasma electrons are ejected to the walls, leaving in the waveguide an uncompensated ion charge which forms a potential well where the remaining electrons oscillate in the pulse field. Due to the decreased group velocity of the wave, these trapped electrons have sufficient time to collide with ions, while their regular oscillatory motion becomes chaotic and thermal. Almost all the energy of the electromagnetic pulse is transferred to the kinetic energy of the electrons. This mechanism of absorption is absent when the pulse power is low, and a potential well does not form in the waveguide.

Published under an exclusive license by AIP Publishing. <https://doi.org/10.1063/5.0052963>

I. INTRODUCTION

The theory of electromagnetic (e/m) field interaction with plasmas goes back to the 1950s with growing interest, from radio wave reflections from the ionosphere and other radio astronomical phenomena to interest in plasma heating for fusion.^{1–4} Generally, when a plane e/m wave is normally incident on a plasma slab of density varying with distance, z , the collisionless plasma can be regarded as a medium with a dielectric constant,

$$\varepsilon(z) = 1 - \frac{\omega_p^2(z)}{\omega^2}, \quad (1)$$

where $\omega_p(z)$ is the plasma frequency and ω is the frequency of the e/m wave. The interaction of an e/m wave with a plasma characterized by this description can be solved analytically in many circumstances when ε is a simple function of z , that is, a nonuniform plasma with density increasing in z to critical ($\varepsilon = 0$).³ The solution describes an oscillating field penetrating the plasma with increasing amplitude. For normal incidence, the amplitude reaches its maximal value at the location where $\omega = \omega_{pe}$, and the wave is then partially transformed into plasma electron oscillations. Thus, the electromagnetic wave transfers its energy to the energy of oscillating electrons.^{5–9}

In recent years, sub-nanosecond pulsed super-radiant backward wave oscillator (SR-BWO) type high power microwave (HPM) sources have become available.^{10,11} We have built two SR-BWO sources, producing 0.5–1.5 GW maximum power, ~ 0.4 ns full width half maximum (FWHM) pulses at ~ 10 GHz (Ref. 12) and ~ 25.5 GHz.¹³ The

interaction of such HPM pulses with plasmas is an uncharted regime, and it may be considered as a downscale of intense ultra-short laser-plasma interaction experiments that is more affordable for a university laboratory and less complicated to diagnose. For example, we anticipated by numerical simulations the HPM induced periodic plasma density modulations and wake fields.¹⁴ Recently, we confirmed these predictions experimentally.¹⁵ In our other experiment, when the HPM pulse focused in a neutral gas, a cylindrical plasma channel is generated which leads the HPM pulse itself propagated for a long distance without a dispersion from the focal region.¹⁶ We identified this observation with ionization induced self-channeling which was predicted theoretically many years before¹⁷ but never observed. This mechanism relies on the fact that the electron impact ionization cross section is maximal at a certain electron energy, which for a Gaussian shaped focal region is not on axis but at a certain distance from it where an over-critical density plasma is formed.

In this paper, we present a new experimental observation when an ~ 1 GW, 0.4 ns, 25.5 GHz HPM pulse is injected in a plasma filled cylindrical waveguide. When the waveguide cutoff frequency, which depends on the plasma density, is close to the microwave frequency, the pulse is completely absorbed and almost no reflected or transmitted power is observed. Such absorption of the HPM pulse in a plasma filled waveguide has not been observed before. These observations are reproduced in particle in cell (PIC) simulations using the Large Scale Plasma (LSP) code^{18,19} and explained by nonlinear interaction of the HPM pulse with the plasma.

II. THE EXPERIMENTAL SETUP AND DIAGNOSTICS

The experimental setup is shown in Fig. 1. The microwave source is an SR-BWO,¹³ generating an ~ 1.2 GW, ~ 0.4 ns, 25.5 GHz HPM pulse. This SR-BWO is driven by a ~ 2 kA hollow electron beam produced by magnetically insulated hollow diode supplied by a ~ 320 kV, ~ 5 ns pulse generated by an all-solid state, high-voltage generator.¹² At the exit of the SR-BWO's slow wave structure, a calibrated coupler²⁰ (Coupler #1) [see Fig. 1(a)] measures the time dependent HPM's field. The HPM traverses a waveguide (~ 800 mm long and 15 mm diameter) installed inside a 160 mm diameter stainless steel tube with a flashboard plasma source placed on its internal wall. At the downstream end of the waveguide, there is a 250 mm long section with 12 longitudinal uniformly distributed slots of 2 mm width, sufficient to allow the plasma to fill the waveguide without HPM power leakage.

The flashboard produced plasma parameters were characterized using different diagnostic methods described in detail in Ref. 13. The time and space-resolved plasma density evolution was measured by visible spectroscopy based on Stark broadening of the H_{β} spectral line and by microwave interferometry. The results of these two methods agreed satisfactorily, demonstrating plasma density uniformity along the waveguide. In addition, the ion plasma density dynamics inside the waveguide was characterized using a biased collimated Faraday cup which was moved inside the waveguide. The data obtained by this Faraday cup agreed with the spectroscopy and microwave interferometry measurements. We estimate a ~ 10 cm longitudinal expansion inside the waveguide beyond both ends of the slots until the HPM is switched on. The plasma density is controllable in the range 10^{10} cm^{-3} – 10^{13} cm^{-3} by the time delay between the beginning of the flashboard discharge and the HPM source's high voltage generator operation. At the waveguide output, a second coupler (Coupler #2)

measures the HPM's field exiting from the plasma. Coupler #1 also measures the pulse reflected from the plasma. The signals from Couplers #1 and #2 were acquired by an Agilent DSAX93204A oscilloscope (33 GHz, 80 Gs/s) or an Agilent DSO81204B oscilloscope (12 GHz, 40 Gs/s) when the power of the microwave pulse was measured using Milltech DXP-28 diodes. Note that reproducibility of the microwave pulse's maximum power and width, measured by Coupler #1, was within $\pm 15\%$. This is because the operation of the gas spark switch at the output of the high voltage generator is not completely reproducible. The purpose of this switch is to reduce the timescale of the rise time of the voltage pulse applied to the cathode to a sub-nanosecond level to provide almost simultaneous formation of the explosive emission plasma at the cathode surface, resulting in an azimuthally uniform electron beam with a sharp front. The latter is important for the efficient SR-BWO operation. Thus, we choose only shots with almost identical waveforms of the microwave pulse registered by Coupler #1.

A 2 mm diameter plastic optical fiber (Edmund Optics Inc.) with its frontal end covered by aluminum (Al) foils of various thicknesses, coupled to a fast (~ 0.5 ns rise time) photo-multiplier-tube (PMT) (Hamamatsu R7400U), is used to detect electron induced luminescence in the fiber. The maximal energy of frontal or radial accelerated electrons was estimated using NIST data.²¹ Radially propagating electron measurements were carried out by a fiber placed at the side of the slotted waveguide [see Fig. 1(a)] and axial electrons by a fiber facing the waveguide on its axis [see Fig. 1(b)]. The fiber was shield by a 1 mm thickness Cu tube to protect it from other possible light sources. A fast-framing intensified camera 4QuikE (Stanford Computer Optics) was used to observe the evolution of the plasma light emission intensity induced by HPM pulse propagating through the waveguide [see Fig. 1(c)].

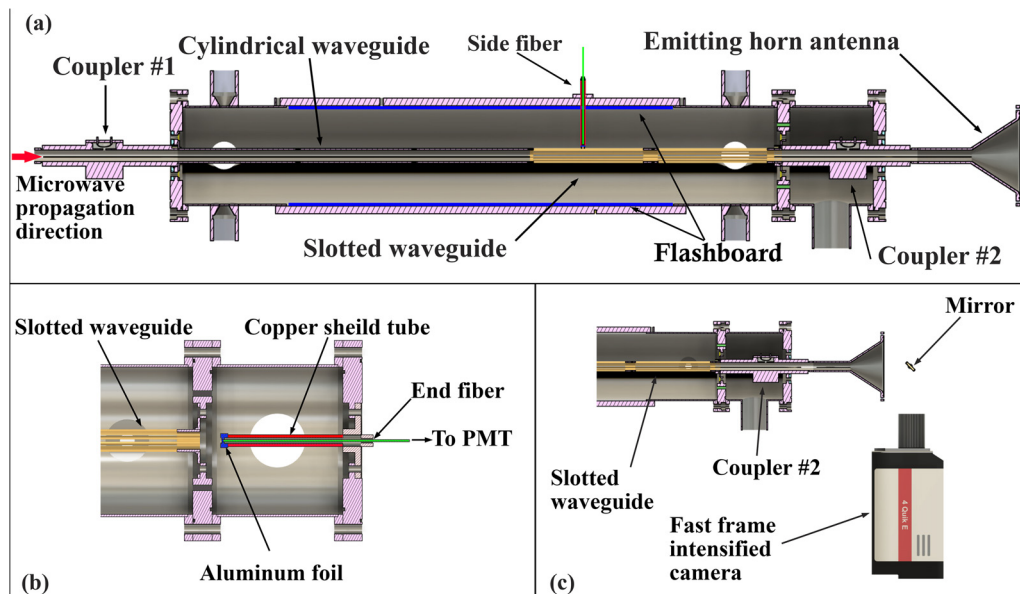


FIG. 1. Schematic drawing of experimental apparatus. (a) Vacuum chamber containing cylindrical waveguide and opening-slots waveguide. Enlarge right side end of (a), with either (b) a frontal fiber detector or (c) a 4QuikE camera, observing the waveguide cross section's plasma light pattern through a 45° placed 2-in. mirror placed at the exit of emitting horn.

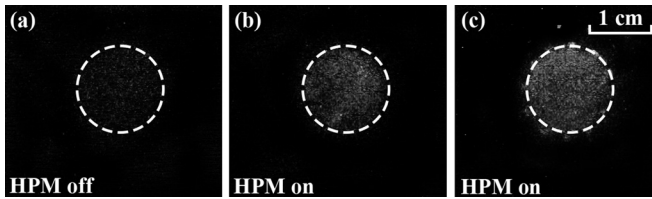


FIG. 2. The incident, transmitted, and reflected HPM pulse registered in (a) vacuum and at (b) $(3 \pm 1) \times 10^{12} \text{ cm}^{-3}$, (c) $(5 \pm 1) \times 10^{12} \text{ cm}^{-3}$, and (d) $(8 \pm 1) \times 10^{12} \text{ cm}^{-3}$ plasma densities.

Two turbo-molecular pumps were used to keep a background pressure of $\sim 7 \times 10^{-3} \text{ Pa}$ in the entire experimental system. When operating the flashboard discharge, the pressure in the flashboard tube increased up to $\sim 4 \text{ Pa}$, measured by a calibrated Penning probe installed inside this tube. This increase in pressure is caused by intense gas desorption from and surface erosion of the flashboard operation.¹⁵

III. EXPERIMENTAL RESULTS

A. The transmitted and reflected MW pulse near the cutoff region

In Fig. 2, one can see the incident, transmitted, and reflected power signal of the HPM pulses registered by the two couplers in vacuum and at various plasma densities. In vacuum [see Fig. 2(a)], the maximum transmitted power decreased ($\sim 25\%$), while the pulse width increased. At the same time, almost no energy is lost (see Fig. 3). Simulation of a Gaussian HPM pulse traversing a slotted waveguide of

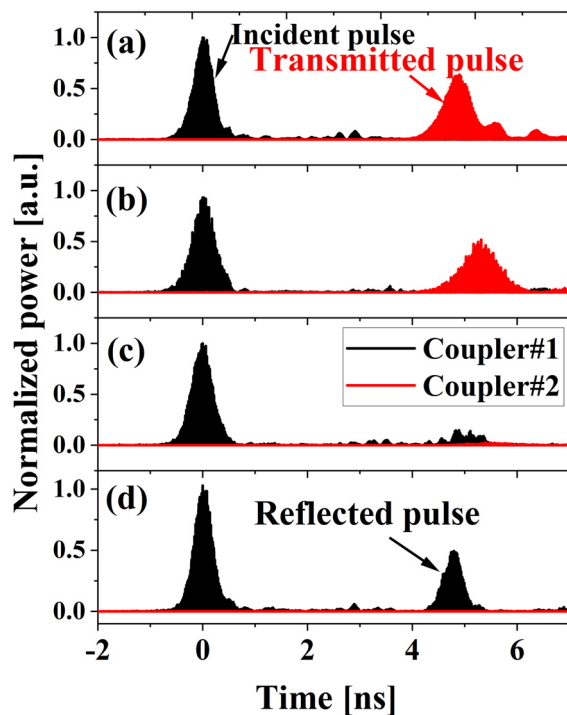


FIG. 3. Transmission (blue) and reflection (red) coefficients for HPM pulses at various plasma densities.

almost the same geometry as in the experiment also showed little energy loss. For a plasma density of $(3 \pm 1) \times 10^{12} \text{ cm}^{-3}$, there are no reflections, and the transmitted power signal is lower and wider [Fig. 2(b)]. At $(5 \pm 1) \times 10^{12} \text{ cm}^{-3}$ [Fig. 2(c)], we observe very small reflection and negligible transmission, and these small amplitude traces are smeared in time. At the slightly higher plasma density of $(8 \pm 1) \times 10^{12} \text{ cm}^{-3}$ [Fig. 2(d)], only the reflected pulse appears. All the plasma densities considered are close to critical $[8 \times 10^{13} \text{ cm}^{-3}$ as defined by Eq. (1)]. Even at the plasma density of 10^{13} cm^{-3} , the maximum of the reflected HPM power is less than 50% of the incident power.

We define transmission and reflection coefficients as the ratio of the energy contained in the transmitted and reflected signals, respectively, normalized to the energy contained in the HPM pulse incident at Coupler #1. The dependence of these experimentally measured transmission and reflection coefficients on plasma density is shown in Fig. 3. One can see that at the plasma density of $(5 \pm 0.5) \times 10^{12} \text{ cm}^{-3}$, the transmitted and reflected coefficients are both very low. This indicates almost complete absorption of the HPM pulse by the plasma. With increasing plasma density, the reflection coefficient increases, but a rather strong absorption is still evident.

The time-frequency spectrum of the incident and transmitted HPM pulse for $(3 \pm 1) \times 10^{12} \text{ cm}^{-3}$ density plasma is shown in Fig. 4. We observe a frequency upshift in the transmitted pulse relative to the frequency of the incident pulse. This frequency upshift can be explained by the increase in plasma density due to additional ionization of plasma ions and background gas by electrons accelerated by the HPM pulse. The neutral gas density can reach $n_0 \approx 8 \times 10^{14} \text{ cm}^{-3}$ due to the operation of the flashboard. The additional ionization introduced by an HPM pulse in a plasma of density $n_e \approx 3 \times 10^{12} \text{ cm}^{-3}$ at this background neutral gas density can be roughly estimated as $n_{pl} \approx n_0 n_e \sigma V t \approx 8 \times 10^{10} \text{ cm}^{-3}$, assuming an ionization cross section $\sigma \approx 10^{-16} \text{ cm}^2$ and an electron velocity of $V \approx 10^9 \text{ cm/s}$ and $t \approx 0.5 \text{ ns}$.

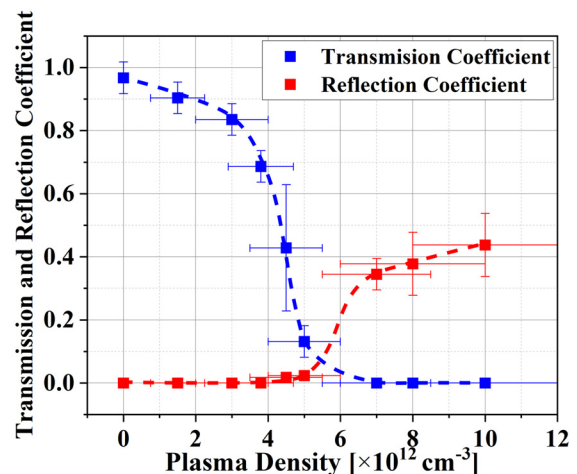


FIG. 4. (a) HPM electric field signal, (b) HPM power signals and average power, and (c) the time-frequency spectrum for the incident (red) and transmitted (blue) pulses for plasma density $(3 \pm 1) \times 10^{12} \text{ cm}^{-3}$.

B. Plasma light emission

A typical plasma light pattern in the presence/absence of the HPM pulse for an initial plasma density of $\sim 3 \times 10^{12} \text{ cm}^{-3}$ is shown in Fig. 5. These fast frame images were taken with an exposure duration of 5 ns. The camera was focused at the center of the slotted region of waveguide. The dashed line shows the inner boundary of the waveguide. One can see that the luminosity of the plasma increases when the HPM pulse is turned on. Increase in light intensity can be related to increase in the plasma electron energy and additional ionization/excitation of the background plasma ions and neutrals. For the plasma density of $8 \times 10^{12} \text{ cm}^{-3}$, the light emission intensity increases [Fig. 5(c)]. Note that for this density, the reflected HPM pulse contains only $\sim 45\%$ of the input HPM pulse [see Fig. 2(d)], leaving 60% of its energy in the plasma as electron kinetic energy. As the plasma density decreased $< 10^{12} \text{ cm}^{-3}$, the light intensity decreased and it could no longer be collected even with longer ($> 20 \text{ ns}$) frame exposure. This is because the plasma becomes increasingly transparent to the HPM.

C. Energetic electrons

Energetic electrons have been detected in the radial direction with the side fiber [see Fig. 1(a)] covered by Al foils of varying thickness. Typical PMT waveforms of the electron induced light in a fiber for plasma density $\sim 3 \times 10^{12} \text{ cm}^{-3}$ are shown in Fig. 6(a). Waveforms of the light emission registered by the PMT for a fixed Al foil thickness of $45 \mu\text{m}$, and different plasma densities are shown in Fig. 6(b). For a

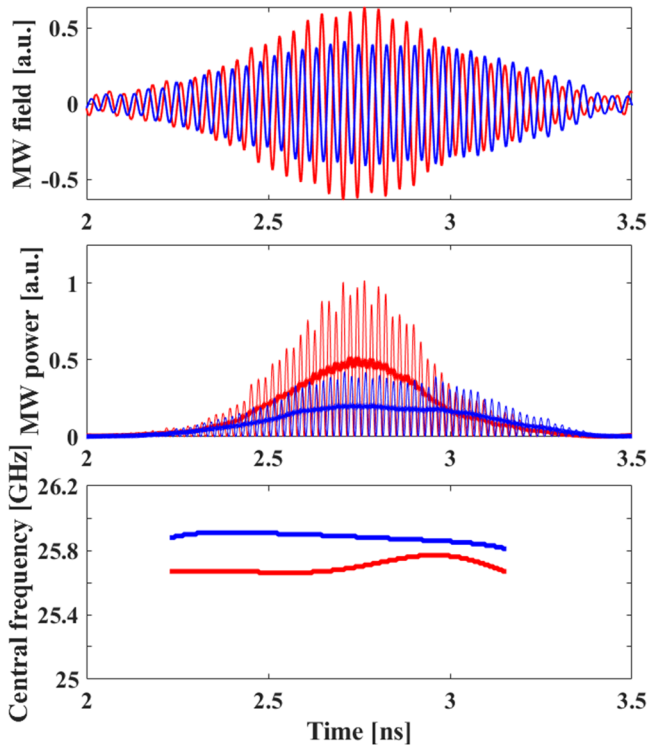


FIG. 5. Fast framing images taken by the 4QuikE fast framing intensified camera (a) in the absence of the HPM pulse and (b) when the HPM pulse is applied with plasma density $\sim 3 \times 10^{12} \text{ cm}^{-3}$ and (c) $\sim 8 \times 10^{12} \text{ cm}^{-3}$.

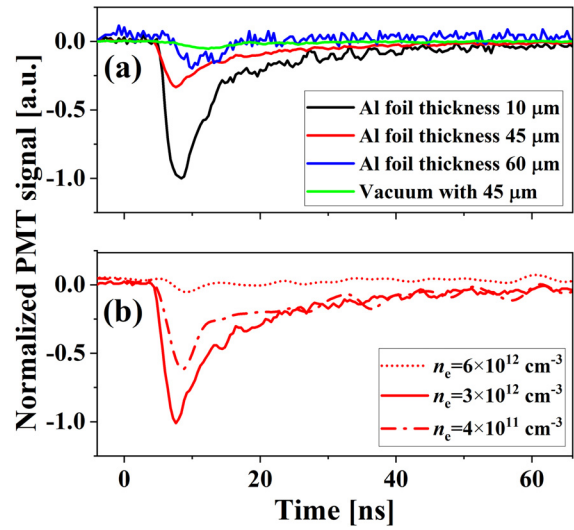


FIG. 6. Normalized (a) PMT signals of light emission induced by energetic electrons collected by the side fiber for various Al foil thicknesses and $n_e \sim 3 \times 10^{12} \text{ cm}^{-3}$ and (b) for a fixed Al foil thickness of $45 \mu\text{m}$ for different plasma densities.

$n_e \sim 3 \times 10^{12} \text{ cm}^{-3}$, energetic electrons have been detected in up to $60 \mu\text{m}$ thickness Al foils. For $90 \mu\text{m}$ thickness, the light intensity was almost equal to the background noise. Thus, we conclude that the maximal energy of radially accelerated electrons for this case does not exceed 100 keV .²¹ $45 \mu\text{m}$ thick Al foils corresponds to $\leq 70 \text{ keV}$ electron energies. Figure 6(b) shows that the appearance of such electrons is maximal for a plasma of $\sim 2 \times 10^{12} \text{ cm}^{-3}$ density. As the density increase to $4 \times 10^{12} \text{ cm}^{-3}$ almost no signal is detected and the same for densities $\geq 5 \times 10^{12} \text{ cm}^{-3}$ [not shown in Fig. 6(b)] even when the thickness was decreased to $10 \mu\text{m}$, indicating the absence of electrons with $\geq 30 \text{ keV}$ energy. Also, one can see that for low plasma densities, $\leq 4 \times 10^{11} \text{ cm}^{-3}$, the presence of electrons with energy $\leq 70 \text{ keV}$ decreases.

In Fig. 7, the light emission induced in the end axial fiber [Fig. 1(b)] covered by a $40 \mu\text{m}$ thick Al foil (electron energies $> 75 \text{ keV}$)²¹

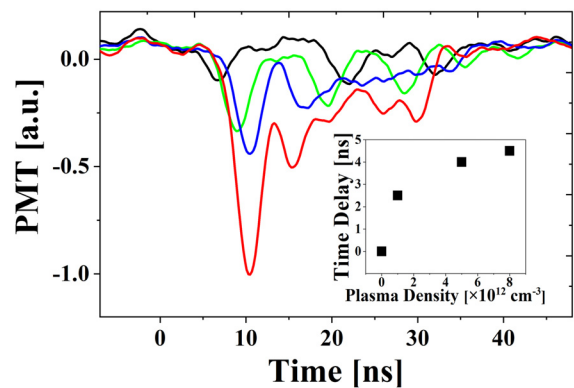


FIG. 7. Normalized signal measured by the PMT coupled to the end axial fiber [see Fig. 1(b)] covered by a $40 \mu\text{m}$ Al foil for various plasma densities and (insert) the time delay of the PMT signal in plasma compared relative to vacuum. (Black) vacuum, (green) $(1 \pm 0.5) \times 10^{12} \text{ cm}^{-3}$, (blue) $(4.5 \pm 1) \times 10^{12} \text{ cm}^{-3}$, and (red) $(7 \pm 1.5) \times 10^{12} \text{ cm}^{-3}$.

for various plasma densities is presented. Note that, in contrast to radially accelerated electrons, as n_e increases, the signal amplitude due to axially accelerated electrons increases as well.

IV. NUMERICAL SIMULATIONS

The cutoff frequency ω_0 of a plasma-filled waveguide reads as $\omega_0 = \sqrt{c^2 k_{\perp}^2 + \omega_{pe}^2}$, where $k_{\perp} = j_{01}/r_{\text{wg}} = 3.2$, $j_{0,1} = 2.4$ is the first zero of the Bessel function, and $\omega_{pe} = (4\pi e^2 n/m_e)^{1/2}$ is the plasma electron frequency. The pulse frequency ω coincides with the cutoff frequency when $n \approx 5 \times 10^{12} \text{ cm}^{-3}$.

We performed 3D PIC simulations of the experimental situation described in Sec. II using the LSP code for a neutral cold collisionless plasma placed in a 100 cm long perfectly conducting solid wall (no slots) waveguide. A 0.86 GW, 25.5 GHz, ~ 0.4 ns Gaussian HPM pulse

with a total energy of 0.19 J is fed at $z=0$ and propagates along the axis z in the TM_{01} mode. Constant density plasma fills this waveguide in the region $z=55\text{--}80$ cm corresponding to the location of the slots. To simulate experimental conditions, the plasma density gradually rises along 10 cm from $z=45$ cm, and it decreases from $z=80$ cm along 10 cm. The plasma consists of electron macroparticles and non-moving positive ions of equal initial density. Locations $z=0$ and 100 cm correspond to the position of the couplers #1 and #2, respectively. In Figs. 8(a)–8(c), the input power signal at $z=0$ cm (blue) and the power signal at $z=100$ cm (red) are drawn for increasing densities. Negative values measured at $z=0$, after a delay time, represent the reflected power from the plasma. When the cutoff frequency is below the pulse frequency, $n = 4 \times 10^{12} \text{ cm}^{-3}$ [Fig. 8(a)], the pulse traverses the plasma without reflections, but its FWHM reduces from 0.42 ns at $z=0$ cm to 0.21 ns at $z=100$ cm and the maximum amplitude

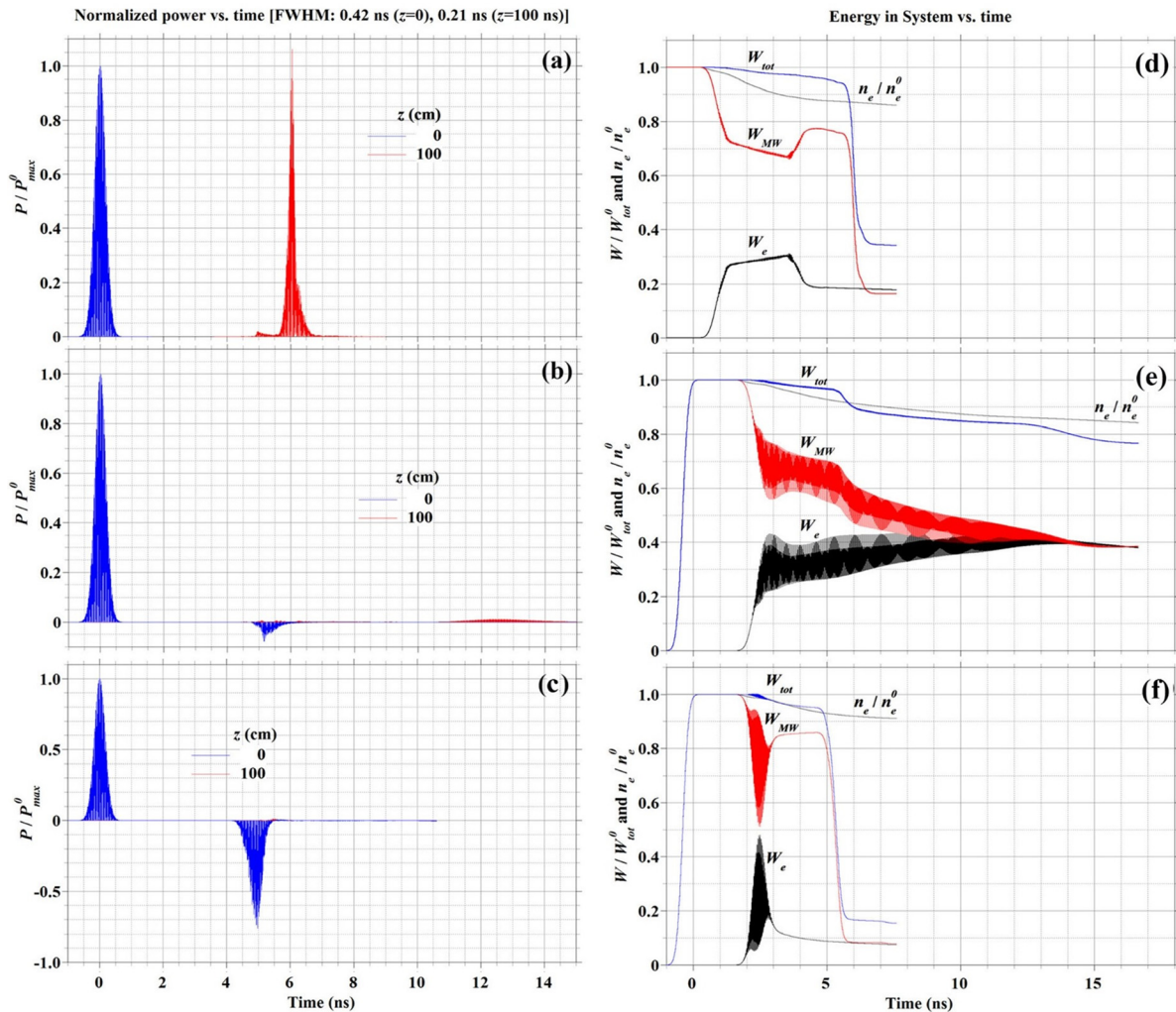


FIG. 8. (a)–(c) The time dependent power signal, P , at $z=0$ (blue) and $z=100$ cm (red) normalized to the maximum power amplitude at $t=0$, P_{max}^0 . (d)–(f) The total energy in the system, W_{tot} (blue), the energy contained in the fields, W_{MW} (red), and the kinetic energy of the electrons, W_e (black), as a function of time. All energies are normalized to the maximum energy input into the system by the HPM pulse, W_{tot}^0 . The ratio between the number of electrons in the system, n_e , and the initial number of electrons, n_e^0 , as a function of time (gray) is drawn on the same scale. The plasma density is $4 \times 10^{12} \text{ cm}^{-3}$ in (a) and (d), $5 \times 10^{12} \text{ cm}^{-3}$ in (b) and (e), and $8 \times 10^{12} \text{ cm}^{-3}$ in (c) and (f).

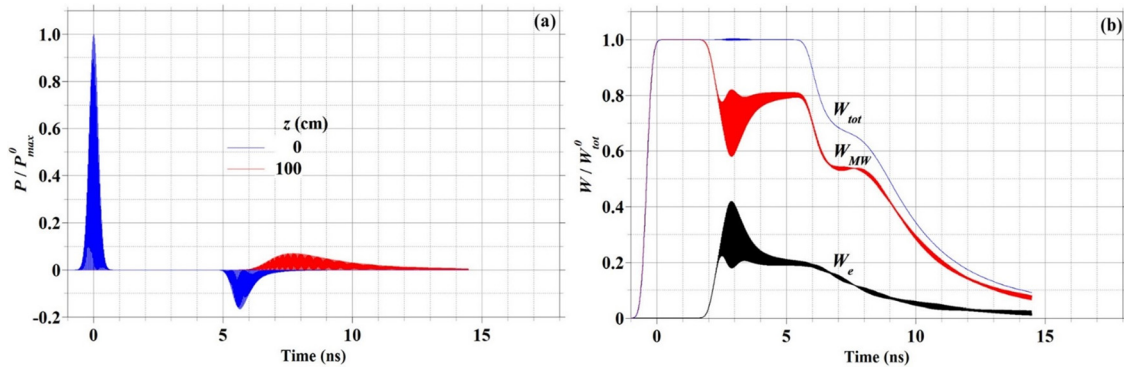


FIG. 9. Same as Figs. 8(b) and 8(e), respectively, for plasma density $5 \times 10^{12} \text{ cm}^{-3}$ but maximal power 8 W.

increases. When the cutoff and the pulse frequencies are almost equal, $n = 5.0 \times 10^{12} \text{ cm}^{-3}$ [Fig. 8(b)], a small ($\sim 5\%$) reflection appears and a very small and smeared transmitted power appears at $z = 100 \text{ cm}$ after a very long time-delay. This behavior is comparable to that observed in Fig. 2(c). As the density increases further (cutoff frequency exceeds the pulse frequency) [see Fig. 8(c)], no transmission is obtained but the reflection becomes powerful and the reflected power shape becomes closer to the input power. The number of electrons present in the system normalized to its initial value is also drawn [Figs. 8(e) and 8(f)]. Electrons accelerated to the waveguide wall gradually leave the system contributing to the decrease in the total energy. The total energy present in the volume occupied by plasma (blue) and this energy separated into that contained in the fields (red) and the kinetic energy of the electrons (black) as function of time are drawn in Figs. 8(d)–8(f). When the pulse reaches the plasma at $z = 45 \text{ cm}$, and as it propagates toward the region of constant plasma density, the energy, W_{MW} , contained in the HPM pulse decreases and the plasma electrons gain kinetic energy, W_e . For the density $4 \times 10^{12} \text{ cm}^{-3}$ in Fig. 8(d), the electron energy increases, while the field energy decreases and there are very small energy exchange oscillations between W_{MW} and W_e . As the pulse exits the plasma, the energy of the electrons decreases, while the field energy increases. This is followed by the decrease in the field energy as the pulse leaves the volume occupied by plasma, and both the electron and field energy become nearly constant. For the density of $5 \times 10^{12} \text{ cm}^{-3}$ [Fig. 8(e)] for which little reflection and almost no transmission is observed, the energy, instead of being reflected or transmitted, oscillates between the electrons and the fields for a long time until it relaxes to a constant, almost equal, field and electron kinetic energy. For the density of $8 \times 10^{12} \text{ cm}^{-3}$ [Fig. 8(f)], the plasma becomes reflective with some energy remaining in the plasma and strong energy exchange oscillations which relax fast.

In Fig. 9, we show the HPM power and energies dependencies for maximal input microwave pulse power of 8 W compared to 0.86 GW in Figs. 8(b) and 8(e) for the same initial plasma density. At this low power, the electron energies quiver, and no electrons are lost to the walls. The transmission and reflection of the microwave pulses is not negligible, but the pulses are somewhat smeared. Also, there are no long-time oscillations and only $\sim 10\%$ of the energy remains in the plasma at $t \sim 15 \text{ ns}$, compared to $\sim 40\%$ for the high-power pulse [see Fig. 8(e)]. In Fig. 10, the calculated transmission and reflection

coefficients for HPM conditions are compared to the experimentally measured values (Fig. 3). One can see that the transmission coefficients agree quite well with the experimental data. Both show nearly complete absorption near the same plasma density of $\sim 5 \times 10^{12} \text{ cm}^{-3}$ below critical ($8 \times 10^{12} \text{ cm}^{-3}$). As the density increases, the experimental reflection coefficients are smaller than those calculated, probably because of energy transfer processes not considered by the simulations, such as nonelastic collisions.

In Fig. 11, we draw the amplitude of the electric field E_z along z on axis at various times for the plasma density $5 \times 10^{12} \text{ cm}^{-3}$. Here we picked times where the oscillating electric field of the HPM pulse is positive. The maximum amplitude of $E_z \sim 500 \text{ kV/cm}$ remains unchanged as the HPM pulse propagates in vacuum. When the pulse enters the plasma and propagates to $z \approx 55 \text{ cm}$, its wavelength increases ~ 6 times. The slowly propagating pulse reaches the edge of the constant density region at $t \approx 11 \text{ ns}$, and it does not propagate further downstream. From the data in Fig. 11, the group velocity of this pulse can be estimated to decrease from $\sim 4 \times 10^9 \text{ cm/s}$ ($55 \text{ cm} < z < 65 \text{ cm}$)

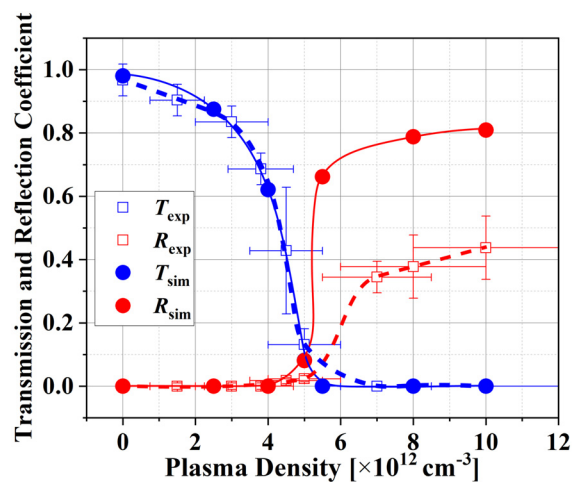


FIG. 10. Comparison of the simulated and experimental (Fig. 3) transmission and reflection coefficients for various plasma densities.

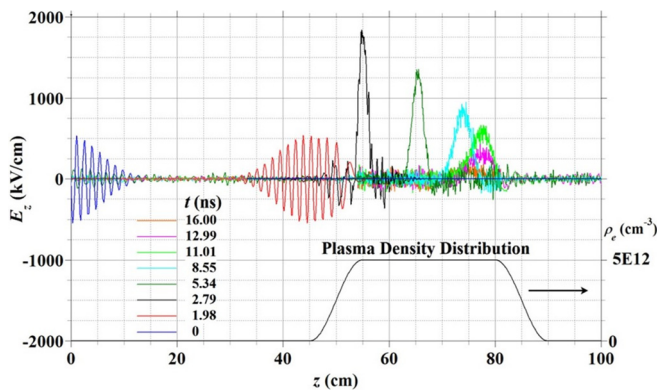


FIG. 11. Electric field E_z vs z ($r=0$) at various times and the initial plasma density vs z .

to $\sim 1.2 \times 10^9$ cm/s ($74 \text{ cm} < z < 77 \text{ cm}$). For the TM_{01} mode, E_r is maximal close to the waveguide wall, i.e., at $r \sim 5.5$ mm; its amplitude also reaches ~ 500 kV/cm, but this value reduces as the pulse propagates through the plasma.

We also simulated the case of a slotted waveguide (as in the experiment) for a plasma density of $5 \times 10^{12} \text{ cm}^{-3}$. The results of these simulations were similar to the results obtained so far with respect to transmission and reflection. In these simulations, we detected energetic electrons emitted radially through the slots reaching energies up to ~ 40 keV. In the experiments, energetic electrons of up to 70 keV were observed for a density of $3 \times 10^{12} \text{ cm}^{-3}$. We also observe energetic axially accelerated electrons at the position of the end fiber. These axial electrons reach energies ~ 50 keV, but these electrons start to appear only 10.1 ns after $t=0$ (as defined in Fig. 7), consistent with the time E_z propagates toward the downstream plasma boundary (see Fig. 11). This delay is of the same order as that observed in the experiment (Fig. 7).

The total absorption of a HPM pulse in a plasma filled waveguide, at a density below critical observed in our experiments and confirmed by simulations, cannot be explained by the linear theory of wave absorption which requires that the density increases above its critical value.^{5,6} This phenomenon can be explained by the nonlinear interaction of the HPM pulse with the plasma. In our earlier research,¹⁴ as well as in the present study, it was shown that during the HPM pulse propagation, the ponderomotive forces push part of the electrons toward the waveguide wall. The uncompensated charge of the immobile ions forms a potential well which traps the remaining electrons in the waveguide. These electrons oscillate in this well in the presence of the HPM radial electric field.

For an initial plasma electron density of $n_e^0 = n_i = 5 \times 10^{18} \text{ m}^{-3}$ (n_i is the initial ion density which remains unchanged), the results of simulations [see Figs. 8(b)–8(e)] show that the depth of the well can reach at ~ 15 ns, $\Delta\phi = 0.5\epsilon_0^{-1}e\Delta n r_{\text{wg}}^2 \approx 200$ kV, where $\Delta n \approx 4 \times 10^{17} \text{ m}^{-3}$ is the excess ion density, $r_{\text{wg}} = 7.5 \times 10^{-3} \text{ m}$, $e = 1.6 \times 10^{19} \text{ C}$, and $\epsilon_0 = 8.85 \times 10^{-12} \text{ F/m}$. At this resonance condition, the group velocity of the HPM pulse approaches zero and the pulse remains in the plasma for a long time. Collisions with ions transfer oscillatory energy of the electrons in the chaotic one, and the pulse loses its energy on the heating of the electrons captured in the potential

well. For plasma density smaller than $\sim 5 \times 10^{12} \text{ cm}^{-3}$ [see Figs. 8(a) and 8(d)], a potential well is also formed, but due to fast pulse propagation, the energy of the oscillating electrons follows the evolution of the pulse's electric field. Thus, only low energy electrons remain captured in the potential well, and negligibly small energy is transferred from the HPM pulse to these electrons. When the plasma density is higher than $\sim 5 \times 10^{12} \text{ cm}^{-3}$ [see Figs. 8(c) and 8(f)], the HPM pulse is reflected from the plasma.

V. SUMMARY

We have experimentally demonstrated that an ~ 1 GW, 25.5 GHz, ~ 0.4 ns HPM pulse traversing a plasma filled cylindrical waveguide is completely absorbed at a plasma density below the critical density, that is, no power is reflected or transmitted. PIC simulations confirm these experimental results. The results of simulations show that the microwave energy transforms into electron kinetic energy through nonlinear interaction with the plasma accompanied by loss of part of the electrons to the waveguide walls. The latter results in the formation of a positively charged potential well with oscillating electrons. Anomalous HPM pulse absorption occurs when the group velocity of the pulse approaches zero and the pulse has enough time to transfer its energy due to electron-ion collisions to the electrons trapped in the well. This nonlinear effect does not occur at low power e/m fields, and such complete absorption has not been observed before for HPM pulses. We also found that energetic electrons are ejected from the plasma both radially and longitudinally, reaching energies of ~ 70 keV in the radial direction and above, in the axial direction. These observations were also confirmed by PIC simulations.

ACKNOWLEDGMENTS

The authors are grateful to S. Gleizer and E. Flyat for their technical help without which this research could not have been performed. This study was supported by Pazy Foundation Grant No. 2025988.

DATA AVAILABILITY

The data that support the findings of this study are available from the corresponding author upon reasonable request.

REFERENCES

- B. N. Gershman, V. L. Ginzburg, and N. G. Denisov, *Usp. Fiz. Nauk* **61**, 561 (1957).
- K. G. Budden, *The Propagation of Radio Waves: The Theory of Radio Waves of Low Power in the Ionosphere and Magnetosphere* (Cambridge University Press, 1988).
- R. B. White and F. F. Chen, *Plasma Phys.* **16**, 565 (1974).
- N. G. Denisov, *Sov. Phys. JETP* **4**, 544 (1957).
- V. E. Golant and A. D. Piliya, *Sov. Phys. Usp.* **14**, 413 (1972).
- J. P. Freidberg, R. W. Mitchell, R. L. Morse, and L. I. Rudinski, *Phys. Rev. Lett.* **28**, 795 (1972).
- K. A. Brueckner and S. Jorna, *Rev. Mod. Phys.* **46**, 325 (1974).
- I. V. Igumenshchev, V. N. Goncharov, W. Seka, D. Edgell, and T. R. Boehly, *Phys. Plasmas* **14**, 092701 (2007).
- J. P. Palastro, J. G. Shaw, R. K. Follett, A. Colaitis, D. Turnbull, A. V. Maximov, V. N. Goncharov, and D. H. Froula, *Phys. Plasmas* **25**, 123104 (2018).
- A. A. Eltchaninov, S. D. Korovin, V. V. Rostov, I. V. Pegel, G. A. Mesyats, S. N. Rukin, V. G. Shpak, M. I. Yalandin, and N. S. Ginzburg, *Laser Part. Beams* **21**, 187 (2003).

- ¹¹V. V. Rostov, I. V. Romanchenko, M. S. Pedos, S. N. Rukin, K. A. Sharypov, V. G. Shpak, S. A. Shunailov, M. R. Ul'Masculov, and M. I. Yalandin, *Phys. Plasmas* **23**, 093103 (2016).
- ¹²G. Shafir, A. Shlapakovski, M. Siman-Tov, Y. Bliokh, J. G. Leopold, S. Gleizer, R. Gad, V. V. Rostov, and Y. E. Krasik, *J. Appl. Phys.* **121**, 033301 (2017).
- ¹³Y. Cao, Y. Bliokh, J. G. Leopold, V. Rostov, Y. Slutsker, and Y. E. Krasik, *Phys. Plasmas* **26**, 023102 (2019).
- ¹⁴Y. P. Bliokh, J. G. Leopold, G. Shafir, A. Shlapakovski, and Y. E. Krasik, *Phys. Plasmas* **24**, 063112 (2017).
- ¹⁵Y. Cao, Y. P. Bliokh, J. G. Leopold, A. Li, G. Leibovitch, and Y. E. Krasik, *Phys. Plasmas* **27**, 053103 (2020).
- ¹⁶G. Shafir, Y. E. Krasik, Y. P. Bliokh, D. Levko, Y. Cao, J. G. Leopold, R. Gad, V. Bernshtam, and A. Fisher, *Phys. Rev. Lett.* **120**, 135003 (2018).
- ¹⁷Y. L. Bogomolov, S. F. Lirin, V. E. Semenov, and A. M. Sergeev, *JETP Lett.* **45**(11), 680 (1987).
- ¹⁸D. R. Welch, D. V. Rose, B. V. Oliver, and R. E. Clark, *Nucl. Instrum. Methods Phys. Res., Sect. A* **464**, 134 (2001).
- ¹⁹D. R. Welch, D. V. Rose, M. E. Cuneo, R. B. Campbell, and T. A. Mehlhorn, *Phys. Plasmas* **13**, 063105 (2006).
- ²⁰L. M. Earley, W. P. Ballard, and C. B. Wharton, *IEEE Trans. Nucl. Sci.* **32**, 2921 (1985).
- ²¹M. J. Berger, J. S. Coursey, M. A. Zucker, and J. Chang, *NIST Stand. Ref. Database* **124** (2017).